ACS Photonics

pubs.acs.org/journal/apchd5

Article

Sunscreen-Inspired ZnO/PEG Composites for Flexible Ultraviolet Photodetectors with a Giant On−Off Ratio

Dewei Yang, Hailong Ma, Jiaqi Li, Huajing Fang,* and Huidong Xie*

Cite This: https://doi.org/10.1021/acsphotonics.2c01959

Read Online

ACCESS | Metrics & More | Article Recommendations | Supporting Information

ABSTRACT: Zinc oxide (ZnO) nanomaterials have attracted much attention in UV photodetectors owing to the suitable band gap and high photoelectric conversion efficiency. However, the loose structure of nanomaterials assembled by a low-temperature process cannot meet the mechanical requirements of flexible photodetectors. The high dark current caused by defects in ZnO severely drags down the response performance of photodetectors. To address these issues, we have proposed a novel strategy for constructing flexible photodetectors based on ZnO and poly(ethylene glycol) (PEG) composites. Inspired by the sunscreen, the addition of PEG can enhance the interaction of ZnO nanoparticles, thus improving the film-forming ability and the mechanical endurance of the composites. By coating the ZnO/PEG composite on a common printing paper, the flexible photodetector shows unexpected good performance, such as a high responsivity of 1.77 A·W^{-1} and a large specific detectivity of 3.89 × 10^{13} Jones. Notably, a giant on−off ratio of up to 1.99 × 10^{5} has been achieved by suppression of dark current. The device also exhibits satisfactory mechanical flexibility after long-term bending tests. In addition, the low-cost raw materials and scalable manufacturing processes further expand its application prospects in flexible optoelectronic technologies.

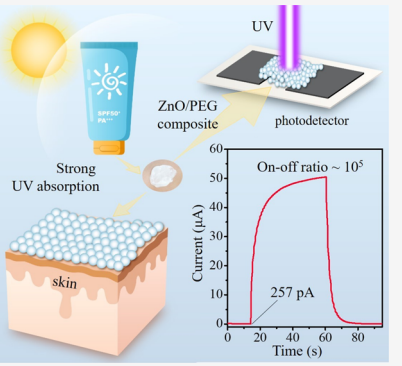

KEYWORDS: *UV photodetector, flexible electronics, ZnO/PEG composite, sunscreen, on−off ratio*

Downloaded via XI'AN JIAOTONG UNIV on March 30, 2023 at 03:16:40 (UTC).
See https://pubs.acs.org/sharingguidelines for options on how to legitimately share published articles.

INTRODUCTION

Ultraviolet (UV) radiation is a class of short-wavelength and high-energy electromagnetic radiation, which has far-reaching effects on organic life.[1−3] Although UV radiation accounts for ∼10% of the total solar radiation, identifying and detecting UV radiation is of great importance to human daily life.[4−6] An ultraviolet photodetector is a kind of sensor that can convert an ultraviolet light signal into an electric signal, which has a wide range of applications in environmental monitoring, geological exploration, space communication, and chemical and pharmaceutical analyses.[7−10] Compared to photodetectors based on rigid substrates, flexible devices can be better shaped and adapted to different curved surfaces. Moreover, the lightweight and portability of flexible photodetectors enable them for new applications in wearable electronics and other high-tech areas.[11−13] For example, Zhou et al. prepared a flexible photodetector based on a halide-exchanged perovskite film, which could be used as a wearable wristband for real-time UV monitoring.[14] Li and co-workers demonstrated a fully flexible Ta-doped β-Ga_2O_3 phototransistor array, which could perform image recognition combined with an artificial neural network.[15] The crucial problem of flexible UV photodetectors lies in the preparation of photosensitive semiconductor materials on flexible substrates. Limited by the poor temperature resistance of flexible substrates such as PET, the high-temperature fabrication process for many inorganic semiconductors is no longer suitable.[16−18] Therefore, it is an urgent pursuit for flexible photodetectors to obtain high-quality semiconductors with excellent photoelectric conversion performance through a low-temperature process.

Among many wide band-gap semiconductors, zinc oxide (ZnO) has a large exciton binding energy of 60 meV and a direct band gap of ∼3.37 eV.[19] The excellent optoelectronic properties as well as the advantages of environmental friendliness, low cost, and no toxicity make zinc oxide an outstanding candidate material for UV photodetectors.[20−23] Compared to the vacuum deposition processes, directly coating nanomaterials on the target substrate does not require expensive equipment and vacuum conditions, allowing for easy mass production and significantly lower production costs.[24−26] However, the loose structure of the film assembled by nanoparticles at low temperatures is easy to disintegrate under mechanical deformation. In addition, the loose structure is not conducive to the transport of photogenerated carriers, which greatly limits the responsivity under illumination. On the other hand, defect-induced carriers widely exist in ZnO nanomaterials, and the resulting high dark current seriously

Received: December 14, 2022

© XXXX American Chemical Society

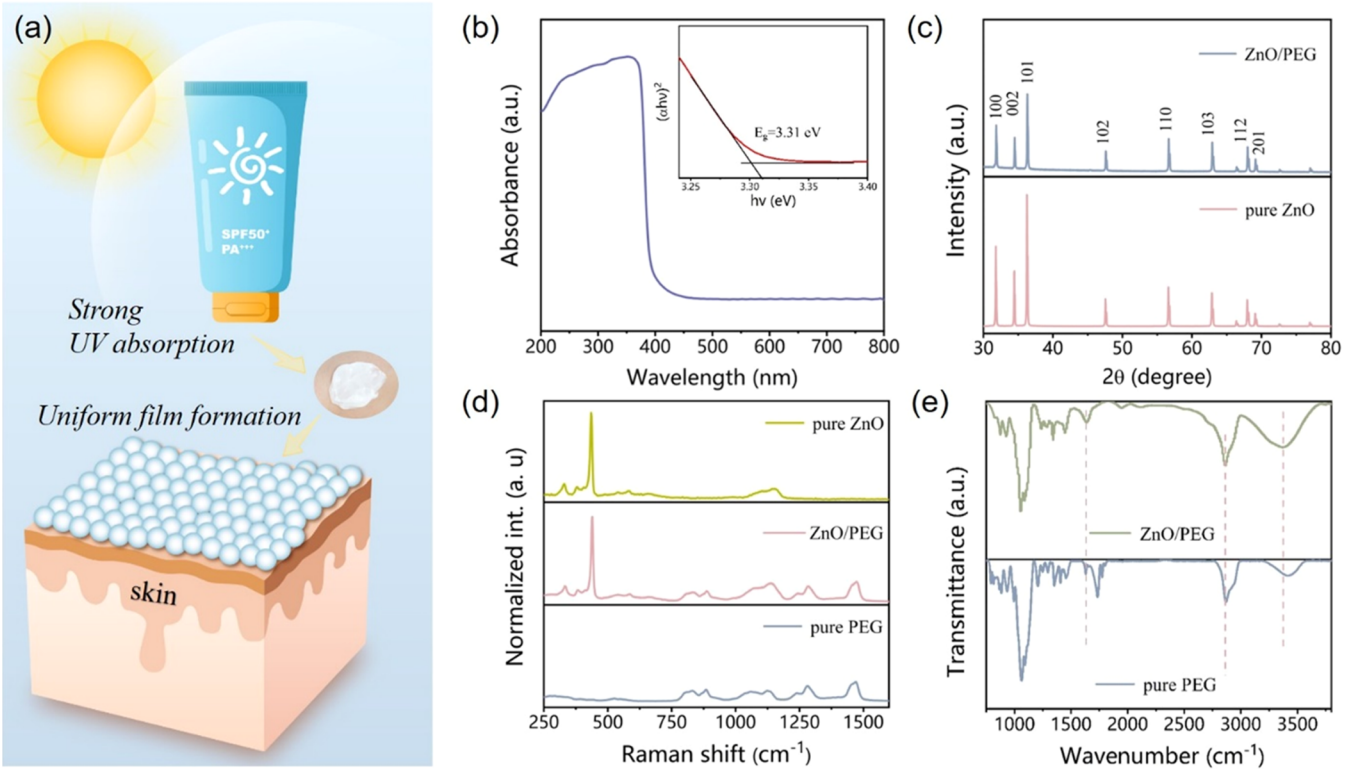

Figure 1. (a) Concept of the ZnO/PEG composite film inspired by the sunscreen. (b) Absorbance spectrum of ZnO nanoparticles; the inset shows the calculated band gap. (c) XRD patterns of ZnO and ZnO/PEG films. (d) Raman spectra of the ZnO/PEG film, ZnO, and pure PEG upon excitation at 532 nm. (e) FTIR spectra of pure PEG and ZnO/PEG films.

impairs the performance of UV photodetectors, leading to unsatisfactory specific detectivity and on−off ratio.[27−29] Thus, challenges remain for fabricating ZnO-based UV photodetectors with both excellent optoelectronic properties and mechanical flexibility.

Coincidentally, zinc oxide nanomaterials are widely adopted in many commercial sunscreens as the core ingredient of UV shielding. The combination of surfactants such as poly(ethylene glycol) (PEG) and its derivatives with ZnO forms a paste material that can be uniformly applied to rough surfaces such as human skin.[30−32] Inspired by the sunscreen, herein, we developed a flexible UV photodetector with excellent performance based on the ZnO/PEG composite film. The PEG polymer chain enhances the interactions between ZnO nanoparticles and improves the film-forming ability so that the composite can be easily applied on flexible substrates. Common printing papers were used as the low-cost flexible substrate and carbon ink was printed as the electrodes. The paper-based photodetector achieves a great responsivity of 1.77 $A{\cdot}W^{-1}$ at 360 nm with a giant on−off ratio of 1.99×10^5. Moreover, it also exhibits good mechanical stability even after 1000 times bending−releasing cycles. This work provides potential candidates for future applications of flexible UV photodetectors.

RESULTS AND DISCUSSION

Long-term exposure to UV radiation can cause skin melanin deposition, produce wrinkles, and even become a major cause of skin cancer.[33−35] Therefore, sunscreen products have been invented to reduce the damage caused by UV radiation to some extent. As shown in Figure 1a, the core ingredients of some sunscreens on the market today include semiconductors such as TiO_2 and ZnO nanomaterials, which have strong absorption of UV light. In addition, PEG and its derivatives were used as emulsifiers and surfactants to facilitate sunscreen coating on the skin. Inspired by this, a homogeneous ZnO/PEG composite film was designed to assemble a flexible paper-based UV photodetector. Here, ZnO nanoparticles were used as the light-sensitive material, and PEG was added in order to obtain a uniform film and improve the adhesion of ZnO nanoparticles on a paper substrate. The optical absorption spectrum of the composite material was first studied because it is the premise of fabricating UV photodetectors. As shown in Figure 1b, the ZnO nanoparticles used in this work have strong absorption in the wavelength range of 200−400 nm, and the strongest absorption peak appears at nearly 360 nm, while the absorption is negligible in visible and IR regions. In order to further investigate the ZnO energy band structure and thus confirm the device operation mechanism, we calculated the band gap (E_g) of ZnO using the *Tauc* plot method of eq 1[36]

$$(\alpha h\nu)^{1/n} = A(h\nu - E_g) \quad (1)$$

where α is the absorbance coefficient, h is the Planck constant, ν is the frequency, A is a constant, the index n is related to the type of semiconductor, and $n = 1/2$ because ZnO is a direct band-gap semiconductor. By plotting $(\alpha h\nu)^{1/n}$ against $h\nu$, the band gap of ZnO nanoparticles in the composite materials is found to be 3.31 eV, which is consistent with that reported by previous work.[37] Through the X-ray diffraction (XRD) examinations of ZnO and ZnO/PEG composite films (Figure 1c), it is not difficult to see that the crystal structure of ZnO in both samples is a hexagonal wurtzite phase. The strong and sharp peaks in XRD indicate that ZnO has high purity and excellent crystallinity. Figure 1d shows the Raman spectra of

https://doi.org/10.1021/acsphotonics.2c01959
ACS Photonics XXXX, XXX, XXX−XXX

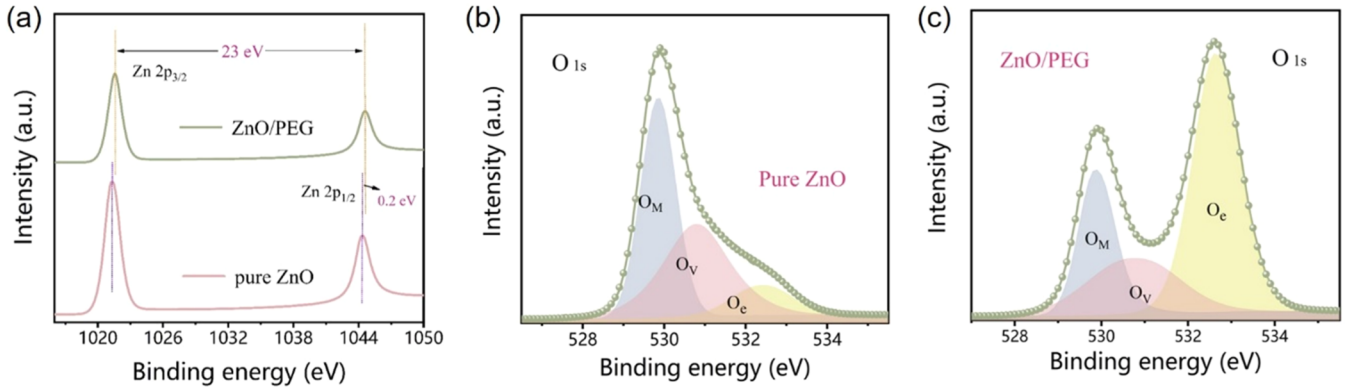

Figure 2. (a) Zn 2p XPS spectra of ZnO and the ZnO/PEG film. The O 1s spectra of (b) ZnO and (c) ZnO/PEG composite film.

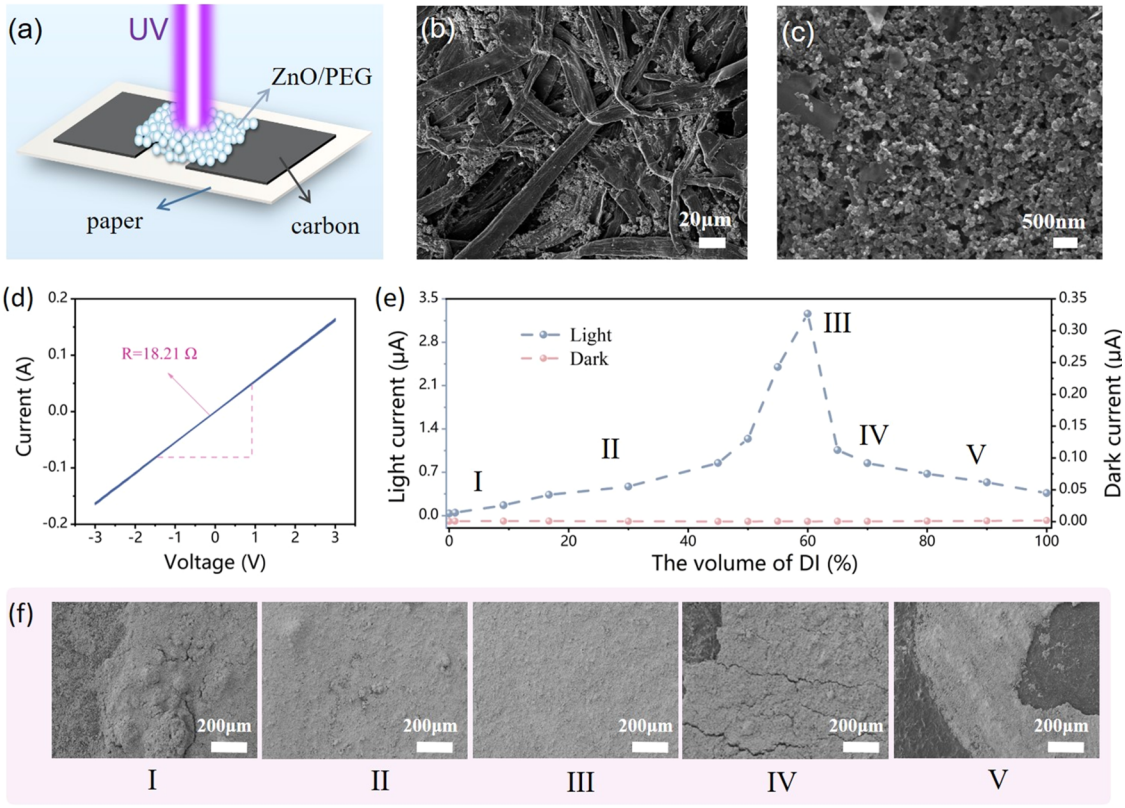

Figure 3. (a) Schematic diagram of the UV photodetector based on the ZnO/PEG composite film and carbon electrodes. (b) SEM image of the A4 printing paper. (c) SEM image of the screen-printed carbon electrode on the printing paper. (d) *I*−*V* curve of the screen-printed carbon electrode on the printing paper. (e) Photoresponse performance of photodetectors prepared with different ZnO/PEG precursors, DI water volume ratios change from 0 to 100% in the dispersions. (f) Morphology of ZnO/PEG films prepared by the precursor with different DI water volume ratios.

each raw material compared with the ZnO/PEG composites. The positions of the Raman peaks and the relative intensities did not change significantly. It is suggested that there is no obvious chemical reaction during the preparation of the composites. The Fourier transform infrared (FTIR) spectrometry results of pure PEG 200 and ZnO/PEG are shown in Figure 1e. The strongest absorption peaks are in the range of 1000−1300 cm^{-1}, which can be attributed to the V_{C-O} bond stretching vibration mode in PEG. The broad peaks at 3200−3500 cm^{-1} in both samples are characteristic of hydrogen bonding.[38] The absorption peak near 3300 cm^{-1} is the O−H stretching vibration of V_{O-H}, and the absorption peaks in 3420−3490 cm^{-1} are attributed to the intramolecular hydrogen bonding connection. The ZnO/PEG composite has a broad absorption peak at 3370 cm^{-1}, and the peak position is red-shifted when compared with pure PEG, indicating an increase in hydrogen bonding in the composite.

In order to investigate the effect of polymer PEG 200 on the surface defects of ZnO nanoparticles, XPS characterization was performed for pure ZnO and ZnO/PEG, respectively. Figure 2a shows high-resolution Zn 2p XPS spectra of ZnO and ZnO/PEG composites. The energy difference between $2p_{3/2}$ and $2p_{1/2}$ is 23 eV, which proves that they both have normal Zn^{2+} chemical valence states.[39] However, the peaks of the ZnO/PEG film shift 0.2 eV toward the high binding energy, illustrating that the electronegativity of oxygen is greater after ZnO combines with PEG. The O 1s spectra of ZnO and ZnO/PEG are shown in Figure 2b,c. The XPS spectra of oxygen can

https://doi.org/10.1021/acsphotonics.2c01959
ACS Photonics XXXX, XXX, XXX−XXX

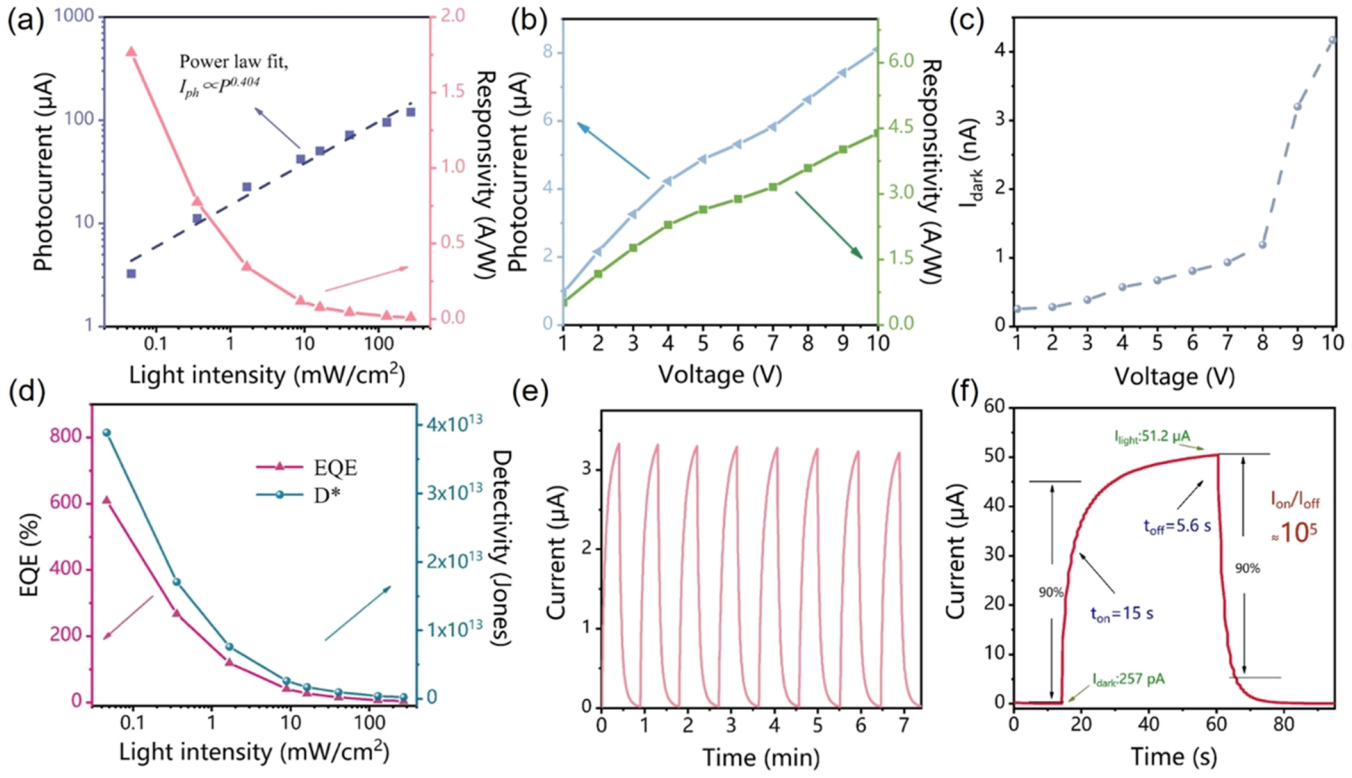

Figure 4. Characterization of device performance with 360 nm UV light. (a) Photocurrent and responsivity as the function of light intensity. (b) Photocurrent and responsivity as the function of the applied voltage. (c) Dark current of the device at different voltages. (d) External quantum efficiency (EQE) and specific detectivity (D^*) of the device at 3 V. (e) Photoswitching characteristics of the paper-based UV photodetector. (f) Response times and the on−off ratio of the ZnO/PEG film UV photodetector.

be deconvolved into three peaks, O_M (530.0 eV), O_V (530.8 eV), and O_e (532.5 eV). The peak located at 530.0 eV (O_M) is the Zn−O bond in the wurtzite structure. The O_V peak originates from oxygen ions near oxygen vacancies in the ZnO lattice. The O_e peak in pure ZnO is sensitive to the sample preparation because this peak corresponds to substances bound on the surface of ZnO nanoparticles.[40] In the ZnO/PEG composite, ZnO nanoparticles are uniformly coated by a PEG polymer, leading to a significantly enhanced O_e peak in Figure 2c. Hence, it can be inferred that PEG is tightly associated with ZnO nanoparticles through hydrogen bonding between the polymer chain and the ZnO surface. In this way, zinc oxide nanoparticles are more easily packed together to form a uniform film on a flexible substrate such as paper. The scanning electron microscopy (SEM) images of the films before and after the addition of PEG are shown in Figure S1, supporting information. It can be found that PEG improves the quality of the films by eliminating cracks. However, no obvious morphological difference is observed in the enlarged view, as shown in Figure S1. This is because the PEG coating layer is very thin. Figure S2 (Supporting Information) shows the TEM image of the PEG-coated ZnO nanoparticle, in which the coating thickness of PEG is only several nanometers. Moreover, the interface between ZnO and the PEG coating layer also worked as the active sites, which can assist in the separation of photogenerated e−h pairs by trapping one of the two carriers.

The paper-based UV photodetector assembled from the ZnO/PEG composite material is shown in Figure 3a. The photodetector consists of a printing paper as a flexible substrate and screen-printed carbon ink as electrodes. As the SEM image in Figure 3b shows, the printing paper is made of abundant cellulose and has a rough surface. From Figure 3c, it is known that the screen-printed carbon electrode has a porous structure, which might be caused by solvent volatilization during the ink-drying process. The good conductivity of this carbon electrode is proved by the $I-V$ curve and shown in Figure 3d. The resistance is obtained as 18.2 Ω by calculating the slope of the straight line. Such a low resistance ensures that the carbon electrode can be used for electrical connections in the UV photodetectors. Moreover, Kelvin probe force microscopy (KPFM) measurement was also carried out on the screen-printed carbon electrode. The calculation of the KPFM result (Figure S3, supporting information) of the carbon electrode yields a work function of 5.17 eV. Based on the conduction band and the valence band of ZnO,[41] the energy band diagram of the UV photodetector is shown in Figure S4.

Then, we focused on the photosensitive components of the device and optimized the preparation parameters of the ZnO/PEG composites. Our experimental results show that the composition of the precursor has a great influence on the final performance of the device. ZnO nanoparticles and PEG were mixed with a fixed ratio and then added into the DI water/EtOH binary solvent. The component ratio of DI water in the binary solvent was found to be a key parameter of the ZnO/PEG precursor. Figure 3e shows the light and dark currents of the devices prepared from different ZnO/PEG precursors. At a constant bias of 3 V, the light current gradually increases with the increase of the DI water component ratio and reaches the highest value at 60% of the DI water volume ratio. The light current decreases with the increase of the DI water volume

https://doi.org/10.1021/acsphotonics.2c01959
ACS Photonics XXXX, XXX, XXX−XXX

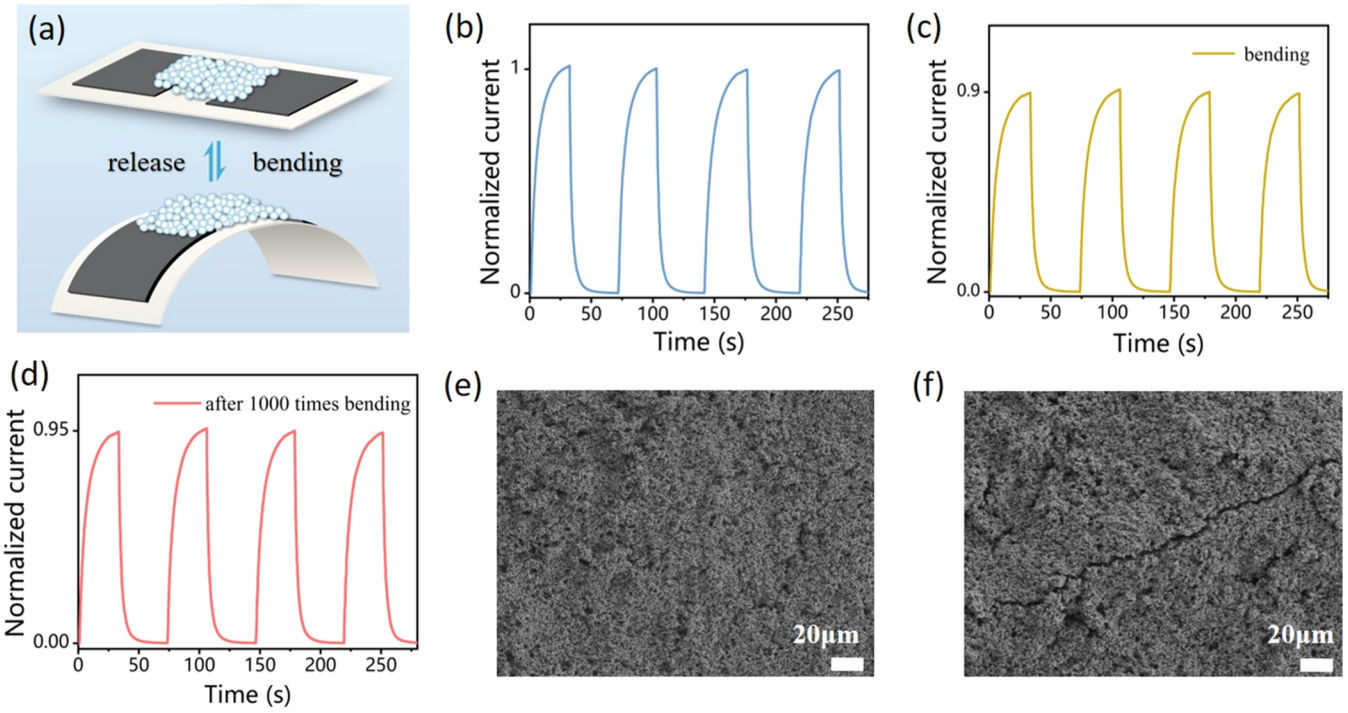

Figure 5. (a) Schematic diagram of the device under bending and releasing states. (b) Normalized current at the initial state. (c) Normalized current at the bending state. (d) Normalized current after 1000 bending−releasing cycles. (e) Surface SEM image of the ZnO/PEG composite film at the initial state. (f) Surface SEM image of the ZnO/PEG composite film at the bending state.

ratio when the volume ratio is more than 60%. The device performance is directly related to the surface morphology of the ZnO/PEG composite film. Corresponding to the value of the light current, Figure 3f shows the SEM images of the composite film fabricated with different DI water/EtOH binary solvents. The ZnO/PEG films prepared with a low DI water volume ratio have a nonuniform dispersion, leading to micron scale aggregation and cracking. Increasing the DI water volume ratio within a certain range can eliminate these undesirable factors. As a result, the best photoresponse performance was obtained with a uniform and dense ZnO/PEG composite film. When the DI water volume ratio is higher than 70% in the binary solvent, cracks appear on the surface of the ZnO/PEG composite film, and even cause the film to peel off from the substrate. This is because excess water molecules can form more hydrogen bonding with PEG molecules, which weakens the interaction between the PEG molecular chain and the ZnO nanoparticles.

With the optimal EtOH/DI water volume ratio in the precursor, we fabricated the ZnO/PEG composite between the carbon electrodes and obtained the low-cost paper-based photodetector. To study the optoelectronic properties of the flexible device, the photocurrents ($I_{ph} = I_{light} - I_{dark}$) at different light intensities were measured at a bias of 3 V. In general, the photocurrent (I_{ph}) resulting from the photogenerated carriers should increase with the increase of incident light intensity (P). The quantitative dependence of the photocurrent (I_{ph}) on the light density is shown in Figure 4a, and their relationship can be fitted as a power law of eq 2[42]

$$I_{ph} \propto P^{\beta} \tag{2}$$

where β is the factor determining the photocurrent response to the light density, which was fitted to be 0.4 in this work. The appearance of this low factor ($0 < \beta < 0.5$) can be attributed to the complex process of device response such as the recombination and trapping of electron−hole pairs. The responsivity (R) is a key criterion for the performance of the photodetector and is calculated from eq 3

$$R = I_{ph}/(S \cdot P) \tag{3}$$

where S is the effective area of the device, that is, the exposed area of the ZnO/PEG composite film between the two carbon electrodes. The responsivity is negatively correlated with the light intensity, and the highest responsivity is calculated to be 1.77 $A \cdot W^{-1}$. Figure 4b shows the relationship between the responsivity and the applied bias. As expected, increasing the bias voltage can directly improve the transport of photogenerated carriers. Both the photocurrent and responsivity increase with the bias, and the maximum responsivity reaches 4.38 $A \cdot W^{-1}$ at a bias of 10 V. However, the dark current also increases as the applied bias gradually increases. It can be seen from Figure 4c, the dark current increases sharply when the applied bias is higher than 8 V. Therefore, we cannot increase the bias voltage without limit in order to get better responsivity. The external quantum efficiency (EQE) and specific detectivity (D^*) are also important parameters of the photodetector, which can be calculated by eqs 4and 5

$$\mathrm{EQE} = (R \cdot h \cdot c)/(\lambda \cdot q) \tag{4}$$

$$D^* = R \cdot \sqrt{S/(2 \cdot q \cdot I_{dark})} \tag{5}$$

where R is the responsivity of the device, h is the Plank constant, c is the velocity of light, λ is the wavelength of the UV laser, q is the elementary charge, and I_{dark} is the dark current. As shown in Figure 4d, both EQE and D^* increase with the decrease of light intensity. Under a weak UV intensity of 4.6×10^{-2} $mW \cdot cm^{-2}$ illumination, the EQE reaches 610% and the specific detectivity reaches 3.89×10^{13} Jones. These values are

https://doi.org/10.1021/acsphotonics.2c01959
ACS Photonics XXXX, XXX, XXX−XXX

comparable to those reported in previous work, which show the excellent photoelectric conversion ability of the ZnO/PEG composite film.[43,44] Under intermittent illumination conditions, the device can output periodically varying currents with a photoswitching behavior. Here, a 360 nm UV laser with an optical chopper was used to generate the intermittent illumination. Figure 4e shows the time-resolved photoresponse of the device at a bias of 3 V. The photocurrent reaches 3.26 μA at a light intensity of 4.6×10^{-2} mW·cm^{-2} and has no attenuation during repetitive operation. In order to measure the response time and on−off ratio, we further investigated the dynamic performance of the paper-based photodetector, as shown in Figure 4f. The rise time of the photodetector is defined as the time required for the device to reach 90% of the equilibrium value upon illumination, and the decay time is defined as the time required to reach 10% of the equilibrium value. For this paper-based photodetector, a rise/decay time of 15/5.6 s was measured at a bias of 3 V. It is worth noting that the steady-state dark current of the photodetector at a 3 V bias voltage is only 257 pA, while the current at a light intensity of 10.15 mW·cm^{-2} reaches 51.2 μA at the equilibrium state. Hence, a giant on−off ratio of 1.99×10^5 was obtained in this paper-based photodetector. We believe that the giant on−off ratio benefits from a special nanostructure inside the ZnO/PEG composite. As mentioned above, PEG polymer chains adhere to the surface of ZnO nanoparticles through the hydroxyl group. Owing to the dielectric property of the PEG layer (with a dielectric constant of 3.6),[45] electrons and holes cannot easily pass through the PEG in the dark state. Hence, the surface-coated PEG chain work as the blocking layers between the adjacent ZnO nanoparticles, which can effectively suppress the dark current. Under UV illumination, electrons in ZnO are excited from the valence band to the conduction band, leading to a large number of photogenerated carriers. These photogenerated carriers can change the energy barrier between PEG and ZnO nanoparticles and increase the probability of interface tunneling. As a result, the photogenerated carriers transport directionally under the external bias to produce a large photocurrent. Based on this interface tunneling effect,[46,47] a giant on−off ratio is realized in ZnO/PEG composite films.

To further investigate the mechanical flexibility of our paper-based photodetector, we measured the photoresponse of the device under bending and releasing states by fixing the device on the acrylic round tube with a diameter of 2 cm, as shown in Figure 5a. Figure 5b,c shows $I-t$ curves of the device before and after bending, and it can be seen that the normalized current decays to 90% of the original value. Figure 5d shows the normalized $I-t$ curve of the paper-based photodetector after 1000 cycles of the bending−releasing test. It can be seen that the current loss after bending 1000 times is only 5%, which indicates that the device has good flexibility as well as stability. Compared to the curve shown in Figure 5c, we found that the photocurrent slightly increased after the device recovered from the bending state to the releasing state. It indicates that mechanical damage of the ZnO/PEG composite film caused by bending can be repaired to a certain extent. In order to explore the intuitive evidence of mechanical damage, we observed the surface morphology of the ZnO/PEG composite film at different states. According to the SEM images of Figure 5e,f, small cracks in the micron scale are generated at the bending state. Without a doubt, these cracks will lead to the obstruction of the carrier migration path and the decrease of the photocurrent. However, composite materials have excellent film-forming ability and tolerance to small cracks, so mechanical damage does not have a fatal effect on the performance of the device.

CONCLUSIONS

In summary, we have successfully demonstrated a high-performance flexible UV photodetector with a printing paper as a low-cost substrate. Inspired by the sunscreen, ZnO/PEG composites with strong UV absorption and excellent film-forming ability have been prepared as photosensitive semiconductor materials. The photodetector based on the ZnO/PEG composite shows an impressive overall performance, including a high responsivity of 1.77 A·W^{-1}, a large specific detectivity of 3.89×10^{13} Jones, and a giant on−off ratio as high as 1.99×10^5. In addition, the UV photodetector maintains 95% of the original photocurrent after 1000 times bending−releasing test, indicating its good mechanical flexibility. The ZnO/PEG composite with low cost and excellent photoelectric properties has a wide application prospect in flexible electronics. Our work not only provides insights into improving the photoelectric response of ZnO nanomaterials but also proposes a simple approach for flexible photodetectors.

EXPERIMENTAL SECTION

Preparation of a ZnO/PEG Precursor. All materials including zinc oxide (ZnO, 99.9%, Forsman), poly(ethylene glycol) (PEG 200, Urchem), A4 printing paper (Deli Group Co., Ltd.), and carbon ink (Jelcon CH-8) were used as received. To prepare A ZnO/PEG precursor, 0.25 g of ZnO nanoparticles and 0.1 g of PEG 200 were added to 3 mL of A DI/EtOH binary solvent and mixed evenly. The binary solvents with different DI volume percentages (from 0 to 100%) were used in the dispersions for comparison.

Device Fabrication. To fabricate a ZnO/PEG UV photodetector, we used an A4 printing paper as a low-cost flexible substrate. The carbon electrodes were coated on the paper by screen printing with carbon ink. The channel length between carbon electrodes was set to be 1 mm. Then, the prepared ZnO/PEG precursor was dropped on the channel and dried at a mild temperature to form a uniform and dense film.

Characterization of Materials and Devices. The surface morphologies of the printing paper, carbon electrode, as well as the ZnO/PEG film were observed by a scanning electron microscope (ZEISS Gemini 500). The crystal structures of the as-prepared ZnO/PEG film were characterized through X-ray diffraction (XRD, Bruker D8-Advance) using Cu Kα radiation. The absorbance spectrum of ZnO was characterized by a spectrophotometer (Perkin Elmer Lambda 1050). The Raman spectra of ZnO and PEG were measured using a Raman spectrometer (LabRAM HR Evolution) with a 532 nm laser. FTIR spectra of pure PEG and the ZnO/PEG film were measured by a Fourier transform infrared spectrometer (FTIR, Nicolet iS 10). The XPS spectra of ZnO and the ZnO/PEG film were tested with an X-ray photoelectron spectrometer (Thermo Fisher ESCALAB Xi+). All of the photoelectric performance tests were carried out through a digital source meter (Keithley 2410). A 360 nm UV laser was used as an illumination source, and the light power was calibrated by an optical power meter (OPHIR photonics, Israel).

https://doi.org/10.1021/acsphotonics.2c01959
ACS Photonics XXXX, XXX, XXX−XXX

■ ASSOCIATED CONTENT

Supporting Information

The Supporting Information is available free of charge at https://pubs.acs.org/doi/10.1021/acsphotonics.2c01959.

SEM images of the film before and after the addition of PEG, TEM images of a PEG-coated ZnO nanoparticle, KPFM image of the carbon electrode, and the energy band diagram of the UV photodetector (PDF)

■ AUTHOR INFORMATION

Corresponding Authors

Huajing Fang − *State Key Laboratory for Mechanical Behavior of Materials, School of Material Science and Engineering, Xi'an Jiaotong University, Xi'an 710049, China;* orcid.org/0000-0002-1939-3700; Email: fanghj@xjtu.edu.cn

Huidong Xie − *School of Chemistry and Chemical Engineering, Xi'an University of Architecture and Technology, Xi'an 710055, China;* orcid.org/0000-0001-5722-0635; Email: xiehuidong@tsinghua.org.cn

Authors

Dewei Yang − *School of Chemistry and Chemical Engineering, Xi'an University of Architecture and Technology, Xi'an 710055, China; State Key Laboratory for Mechanical Behavior of Materials, School of Material Science and Engineering, Xi'an Jiaotong University, Xi'an 710049, China*

Hailong Ma − *State Key Laboratory for Mechanical Behavior of Materials, School of Material Science and Engineering, Xi'an Jiaotong University, Xi'an 710049, China*

Jiaqi Li − *State Key Laboratory for Mechanical Behavior of Materials, School of Material Science and Engineering, Xi'an Jiaotong University, Xi'an 710049, China*

Complete contact information is available at: https://pubs.acs.org/10.1021/acsphotonics.2c01959

Funding

This work was supported by the National Natural Science Foundation of China (No. 51902250).

Notes

The authors declare no competing financial interest.

■ ACKNOWLEDGMENTS

The authors thank Danli Zhang of the Center for Advancing Materials Performance from the Nanoscale (CAMP-Nano) for contributions to the material characterization. The Instrument Analysis Center of Xi'an Jiaotong University is acknowledged for its great help in measurements.

■ REFERENCES

(1) Li, Z. L.; Li, Z. Q.; Zuo, C. L.; Fang, X. S. Application of Nanostructured TiO_2 in UV Photodetectors: A Review. *Adv. Mater.* **2022**, *34*, No. 210908.

(2) Xie, C.; Lu, X. T.; Tong, X. W.; Zhang, Z. X.; Liang, F. X.; Liang, L.; Luo, L. B.; Wu, Y. C. Recent Progress in Solar-Blind Deep-Ultraviolet Photodetectors Based on Inorganic Ultrawide Bandgap Semiconductors. *Adv. Funct. Mater.* **2019**, *29*, No. 1806006.

(3) Kaur, D.; Kumar, M. A Strategic Review on Gallium Oxide Based Deep-Ultraviolet Photodetectors: Recent Progress and Future Prospects. *Adv. Opt. Mater.* **2021**, *9*, No. 2002160.

(4) Wu, L. L.; Fang, H. J.; Zheng, C.; Wang, Q.; Wang, H. A multifunctional smart window: detecting ultraviolet radiation and regulating the spectrum automatically. *J. Mater. Chem. C* **2019**, *7*, 10446−10453.

(5) Polat, E. O.; Mercier, G.; Nikitskiy, I.; Puma, E.; Galan, T.; Gupta, S.; Montagut, M.; Piqueras, J. J.; Bouwens, M.; Durduran, T.; Konstantatos, G.; Goossens, S.; Koppens, F. Flexible graphene photodetectors for wearable fitness monitoring. *Sci. Adv.* **2019**, *5*, No. eaaw7846.

(6) Zhang, Y.; Peng, M.; Liu, Y.; Zhang, T. T.; Zhu, Q. Q.; Lei, H.; Liu, S.; Tao, Y.; Li, L.; Wen, Z.; Sun, X. Flexible Self-Powered Real-Time Ultraviolet Photodetector by Coupling Triboelectric and Photoelectric Effects. *ACS Appl. Mater. Interfaces* **2020**, *12*, 19384−19392.

(7) Fang, H.; Zheng, C.; Wu, L.; Li, Y.; Cai, J.; Hu, M.; Fang, X.; Ma, R.; Wang, Q.; Wang, H. Solution-processed self-powered transparent ultraviolet photodetectors with ultrafast response speed for high-performance communication system. *Adv. Funct. Mater.* **2019**, *29*, No. 1809013.

(8) Zheng, Q. H.; Huang, J.; Cao, S.; Gao, H. L. A flexible ultraviolet photodetector based on single crystalline MoO_3 nanosheets. *J. Mater. Chem. C* **2015**, *3*, 7469−7475.

(9) Shiau, J. S.; Brahma, S.; Huang, J. L.; Liu, C. P. Fabrication of flexible UV-B photodetectors made of $Mg_xZn_{1-x}O$ films on PI substrate for enhanced sensitivity by piezophototronic effect. *Appl. Mater. Today* **2020**, *20*, No. 100705.

(10) Li, T. Y.; Ma, J. L.; Chen, X.; Yan, J. J.; Zhang, M. Y.; Wu, D.; Tian, Y. T.; Li, X. J.; Shi, Z. F. Antisolvent-Processed One-Dimensional Ternary Rubidium Copper Bromine Microwires for Sensitive and Flexible Ultraviolet Photodetectors. *ACS Appl. Mater. Interfaces* **2021**, *13*, 49007−49016.

(11) Zhang, Y. Y.; Zheng, Y. X.; Lai, J. Y.; Seo, J. H.; Lee, K. H.; Tan, C. S.; An, S.; Shin, S. H.; Son, B.; Kim, M. Ultraviolet Photodetectors with Two Dimensional Electron Gas Based on Unconventional Release Strategy. *ACS Nano.* **2021**, *15*, 8386−8396.

(12) Li, D. Y.; Zhou, D. L.; Xu, W.; Chen, X.; Pan, G. C.; Zhou, X. Y.; Ding, N.; Song, H. W. Plasmonic Photonic Crystals Induced Two-Order Fluorescence Enhancement of Blue Perovskite Nanocrystals and Its Application for High-Performance Flexible Ultraviolet Photodetectors. *Adv. Funct. Mater.* **2018**, *28*, No. 1804429.

(13) Guo, D. H.; Yang, L. Q.; Zhao, J. C.; Li, J.; He, G.; Yang, D. Z.; Wang, L. G.; Vadim, A.; Ma, D. G. Visible-blind ultraviolet narrowband photomultiplication-type organic photodetector with an ultrahigh external quantum efficiency of over 1000000%. *Mater. Horiz.* **2021**, *8*, 2293−2302.

(14) Zhou, Y.; Qiu, X.; Wan, Z. A.; Long, Z. H.; Poddar, S.; Zhang, Q. P.; Ding, Y. C.; Chan, C. L. J.; Zhang, D. Q.; Zhou, K. M.; Lin, Y. J.; Fan, Z. Y. Halide-exchanged perovskite photodetectors for wearable visible-blind ultraviolet monitoring. *Nano Energy* **2022**, *100*, No. 107516.

(15) Li, X. X.; Zeng, G.; Li, Y. C.; Zhang, H.; Ji, Z. G.; Yang, Y. G.; Luo, M.; Hu, W. D.; Zhang, D. W.; Lu, H. L. High responsivity and flexible deep-UV phototransistor based on Ta-doped β-Ga_2O_3. *npj Flexible Electron.* **2022**, *6*, 47.

(16) Jang, H.; Kwon, D. K.; Kim, D. H.; Myoung, J. M. Characteristics of flexible ZnO nanorod UV photodetectors processed by using a direct silicon etching transfer method. *J. Mater. Chem. C* **2022**, *10*, 6805−6811.

(17) Peng, M. Z.; Liu, Y. D.; Yu, A. F.; Zhang, Y.; Liu, C. H.; Liu, J. Y.; Wu, W.; Zhang, K.; Shi, X. Q.; Kou, J. Z.; Zhai, J. Y.; Wang, Z. L. Flexible Self-Powered GaN Ultraviolet Photoswitch with Piezo-Phototronic Effect Enhanced On/Off Ratio. *ACS Nano* **2016**, *10*, 1572−1579.

(18) Dong, Y. H.; Zou, Y. S.; Song, J. Z.; Li, J. H.; Han, B. N.; Shan, Q. S.; Xu, L. M.; Xue, J.; Zeng, H. B. An all-inkjet-printed flexible UV photodetector. *Nanoscale* **2017**, *9*, 8580−8585.

(19) Su, M. M.; Zhang, T. L.; Su, J.; Wang, Z.; Hu, Y. M.; Gao, Y. H.; Gu, H. S.; Zhang, X. H. Homogeneous ZnO nanowire arrays p-n junction for blue light-emitting diode applications. *Opt. Express* **2019**, *27*, A1207−A1215.

(20) Park, J.; Lee, J. S.; Noh, Y.; Shin, K. H.; Lee, D. J. Flexible ultraviolet photodetectors with ZnO nanowire networks fabricated by large area controlled roll-to-roll processing. *J. Mater. Chem. C* **2016**, *4*, 7948−7958.
(21) Lee, D. L.; Seol, M. L.; Motilal, G.; Kim, B.; Moon, D. I.; Han, J. W.; Meyyappan, M. All 3D-Printed Flexible ZnO UV Photodetector on an Ultraflat Substrate. *ACS Sens.* **2020**, *5*, 1028−1032.
(22) Wu, J. D.; Lin, L. Y. A Flexible Nanocrystal Photovoltaic Ultraviolet Photodetector on a Plant Membrane. *Adv. Opt. Mater.* **2015**, *3*, 1530−1536.
(23) Wang, H.; Ma, J.; Cong, L.; Zhou, H.; Li, P.; Fei, L.; Li, B.; Xu, H.; Liu, Y. Piezoelectric effect enhanced flexible UV photodetector based on Ga_2O_3/ZnO heterojunction. *Mater. Today Phys.* **2021**, *20*, No. 100464.
(24) Zhu, J.; Hersam, M. C. Assembly and Electronic Applications of Colloidal Nanomaterials. *Adv. Mater.* **2017**, *29*, No. 160389.
(25) Liu, X.; Gu, L. L.; Zhang, Q. P.; Wu, J. Y.; Long, Y. Z.; Fan, Z. Y. All-printable band-edge modulated ZnO nanowire photodetectors with ultra-high detectivity. *Nat. Commun.* **2014**, *5*, No. 4007.
(26) Gonçalves, B. F.; Sadewasser, S.; Salonen, L. M.; Lanceros-Méndez, S.; Kolen'ko, S. L. Y. V. Merging solution processing and printing for sustainable fabrication of Cu(In,Ga)Se_2 photovoltaics. *Chem. Eng. J.* **2022**, *442*, No. 136188.
(27) Wang, P.; Wang, Y.; Ye, L.; Wu, M. Z.; Xie, R. Z.; Wang, X. D.; Chen, X. S.; Fan, Z. Y.; Wang, J. L.; Hu, W. D. Ferroelectric Localized Field-Enhanced ZnO Nanosheet Ultraviolet Photodetector with High Sensitivity and Low Dark Current. *Small* **2018**, *14*, No. 1800492.
(28) Chen, T.; Gao, X.; Zhang, J. Y.; Xu, J. L.; Wang, S. D. Ultrasensitive ZnO Nanowire Photodetectors with a Polymer Electret Interlayer for Minimizing Dark Current. *Adv. Opt. Mater.* **2020**, *8*, No. 1901289.
(29) Young, S. J.; Liu, Y. H.; Chang, S. J.; Chiu, C. F. Fabrication of Silicon Dioxide by Photo-Chemical Vapor Deposition to Decrease Detector Current of ZnO Ultraviolet Photodetectors. *ACS Omega* **2020**, *5*, 27566−27571.
(30) Bocca, B.; Caimi, S.; Senofonte, O.; Alimonti, A.; Petrucci, F. ICP-MS based methods to characterize nanoparticles of TiO_2 and ZnO in sunscreens with focus on regulatory and safety issues. *Sci. Total Environ.* **2018**, *630*, 922−930.
(31) Jeon, S. K.; Kim, E. J.; Lee, J.; Lee, S. Potential risks of TiO_2 and ZnO nanoparticles released fromsunscreens into outdoor swimming pools. *J. Hazard. Mater.* **2016**, *317*, 312−318.
(32) Girigoswami, K.; Viswanathan, M.; Murugesan, R.; Girigoswami, A. Studies on polymer-coated zinc oxide nanoparticles: UV-blocking efficacy and in vivo toxicity. *Mater. Sci. Eng., C* **2015**, *56*, 501−510.
(33) Araki, H.; Kim, J.; Zhang, S.; Banks, A.; Crawford, K. E.; Sheng, X.; Gutruf, P.; Shi, Y.; Pielak, R. M.; Rogers, J. A. Materials and Device Designs for an Epidermal UV Colorimetric Dosimeter with Near Field Communication Capabilities. *Adv. Funct. Mater.* **2017**, *27*, No. 1604465.
(34) Zhou, J.; Chen, L.; Wang, Y.; He, Y.; Pan, X.; Xie, E. An overview on emerging photoelectrochemical self-powered ultraviolet photodetectors. *Nanoscale.* **2016**, *8*, 50−73.
(35) Wu, L.; Fang, H.; Wu, W.; Ma, H.; Zheng, C.; Wang, H. Monolithic integrated multifunctional photoelectrochemical device for smart ultraviolet management. *Mater. Today Energy* **2021**, *20*, No. 100676.
(36) Saleh Al-Khazali, S. M.; Al-Salman, H. S.; Hmood, A. Low cost flexible ultraviolet photodetector based on ZnO nanorods prepared using chemical bath deposition. *Mater. Lett.* **2020**, *277*, No. 128177.
(37) Zhang, W.; Jiang, D. Y.; Zhao, M.; Duan, Y. H.; Zhou, X.; Yang, X. J.; Shan, C. C.; Qin, J. M.; Gao, S.; Liang, Q. C.; Hou, J. H. Piezo-phototronic effect for enhanced sensitivity and response range of ZnO thin film flexible UV photodetectors. *J. Appl. Phys.* **2019**, *125*, No. 024502.
(38) Naskar, A.; Bera, S.; Bhattacharya, R.; Roy, S. S.; Jan, S. Synthesis, characterization and cytotoxicity of polyethylene glycol coupled zinc oxide-chemically converted graphene nanocomposite on human OAW42 ovarian cancer cells. *Polym. Adv. Technol.* **2016**, *27*, 436−443.
(39) Sun, J. H.; Huang, J. H.; Lan, X. Y.; Zhang, F. C.; Zhao, L. Z.; Zhang, Y. Enhancing the performance of blue quantum-dot light-emitting diodes through the incorporation of polyethylene glycol to passivate ZnO as an electron transport layer. *RSC Adv.* **2020**, *10*, 23121−23127.
(40) Parmar, D. H.; Joao, M. P.; Zhu, T.; Maral, V.; Ozan, A.; Margherita, B.; Amin, M. N.; Sjoerd, H.; Edward, H. S. Controlled Crystal Plane Orientations in the ZnO Transport Layer Enable High-Responsivity, Low-Dark-Current Infrared Photodetectors. *Adv. Mater.* **2022**, *34*, No. 2200321.
(41) Wang, Y.; Zhu, L.; Feng, Y.; Wang, Z.; Wang, Z. L. Comprehensive Pyro-Phototronic Effect Enhanced Ultraviolet Detector with ZnO/Ag Schottky Junction. *Adv. Funct. Mater.* **2019**, *29*, No. 1807111.
(42) Fang, H. J.; Ma, H. L.; Zheng, C.; Lennon, S.; Wu, W. T.; Wu, L. L.; Wang, H. A high- performance transparent photodetector via building hierarchical g-C_3N_4 nanosheets/CNTs van der Waals heterojunctions by a facile and scalable approach. *Appl. Surf. Sci.* **2020**, *529*, No. 147122.
(43) Duan, Y. H.; Zhang, S. Q.; Cong, M. Y.; Jiang, D. Y.; Liang, Q. C.; Zhao, X. J. Performance Modulation on MgZnO/ZnO Heterojunction Flexible UV Photodetector by Piezophototronic Effect. *J. Mater. Chem. C* **2020**, *8*, 12917−12926.
(44) Kim, Y.; Kim, J.; Kim, H. M.; Jang, J. Quantum-Dots Photosensor with Wide Bandgap P-Type and N-Type Oxide Semiconductors for High Detectivity and Responsivity. *Adv. Mater. Technol.* **2020**, *5*, No. 1900857.
(45) Liu, D. N.; Wang, J. W.; Peng, W. H.; Wang, X. Z.; Ren, H.; Donald, W. K. The application of organic polyethylene glycol-polyaniline multi-alternating block (more than triblock) copolymer in polymer-based dielectric composites. *React. Funct. Polym.* **2022**, *170*, No. 105139.
(46) Chang, C.-Y.; Pan, F. M.; Lin, J. S.; Yu, T. Y.; Li, Y. M.; Chen, C. Y. Lateral amorphous selenium metal-insulator-semiconductor-insulator-metal photodetectors using ultrathin dielectric blocking layers for dark current suppression. *J. Appl. Phys.* **2016**, *120*, No. 234501.
(47) Zeng, J. P.; Meng, C. F.; Li, X. M.; Wu, Y.; Liu, S. T.; Zhou, H.; Wang, H.; Zeng, H. B. Interfacial-Tunneling-Effect-Enhanced $CsPbBr_3$ Photodetectors Featuring High Detectivity and Stability. *Adv. Funct. Mater.* **2019**, *29*, No. 1904461.

https://doi.org/10.1021/acsphotonics.2c01959
ACS Photonics XXXX, XXX, XXX−XXX